optica

Terahertz-driven, all-optical electron gun

W. Ronny Huang,[1,2] Arya Fallahi,[1] Xiaojun Wu,[1] Huseyin Cankaya,[1] Anne-Laure Calendron,[1] Koustuban Ravi,[1,2] Dongfang Zhang,[1] Emilio A. Nanni,[2] Kyung-Han Hong,[2] and Franz X. Kärtner[1,2,*]

[1]Center for Free-Electron Laser Science at Deutsches Electronen Synchrotron (DESY), Department of Physics and the Center for Ultrafast Imaging, University of Hamburg, Hamburg 22761, Germany
[2]Research Laboratory of Electronics, Massachusetts Institute of Technology (MIT), Cambridge, Massachusetts 02139, USA
*Corresponding author: franz.kaertner@desy.de

Received 27 June 2016; revised 5 September 2016; accepted 14 September 2016 (Doc. ID 267483); published 24 October 2016

Ultrashort electron beams with a narrow energy spread, high charge, and low jitter are essential for resolving phase transitions in metals, semiconductors, and molecular crystals. These accelerated beams, produced by phototriggered electron guns, are also injected into accelerators for x-ray light sources. The achievable resolution of these time-resolved electron diffraction or x-ray experiments has been hindered by surface field and timing jitter limitations in conventional RF guns, which thus far are <200 MV/m and >96 fs, respectively. A gun driven by optically generated single-cycle terahertz (THz) pulses provides a practical solution for enabling not only GV/m surface fields but also absolute timing stability, since the pulses are generated by the same laser as the phototrigger. Here, we demonstrate an all-optical THz gun yielding a peak electron energy approaching 1 keV, accelerated by >300 MV/m THz fields in a micrometer-scale waveguide structure. We also achieve quasi-monoenergetic, sub-kiloelectron volt bunches with 32 fC of charge, which can already be used for time-resolved low-energy electron diffraction. Such ultracompact, easy-to-implement guns—driven by intrinsically synchronized THz pulses that are pumped by an amplified arm of the already-present photoinjector laser—provide a new tool with the potential to transform accelerator-based science.

OCIS codes: (320.0320) Ultrafast optics; (350.4990) Particles.

http://dx.doi.org/10.1364/OPTICA.3.001209

The central challenge of an electron gun is to accelerate electrons from rest to high energies as quickly as possible to avoid the beam-degrading effects of space charge, which scale inversely as the electron energy squared [1] or as the extraction field squared. To achieve these high fields on the surface of the photoemitter, there are currently two types of electron guns, DC and RF guns, which have field limitations of around 10 [2] and 200 MV/m [3], respectively, due to breakdown mechanisms on common accelerator materials [4,5]. Furthermore, RF guns utilize high-power RF fields, which involve large klystrons, pulsed heating issues [4,5], and elaborate synchronization schemes [6,7]. The need for a higher extraction field in a compact electron source, which may ultimately lead to lower-emittance electron bunches [8], has propelled the development of photonic [IR- or terahertz (THz)-driven] linear accelerators (linacs) with promising results [9,10]. However, the potential advantages of photonic linacs have not extended to photonic guns, the initial acceleration stage that is quintessential to determining the final electron beam quality and can benefit most from higher accelerating fields. The difficulty, which lies primarily in phase matching the electromagnetic (EM) wave with nonrelativistic electrons, is greater for short IR wavelengths [11] than for THz radiation, though IR acceleration can occur indirectly via a plasma [12]. Thus, we recently proposed the development of a single-cycle THz gun [13,14] to exploit the GV/m fields possible with optically generated THz sources [15]. Here, we implement such a THz gun. Leveraging the gun's simple geometries and flexible machining requirements, we integrate it into a practical, compact machine that is powered by a 1 kHz, few-millijoule laser and operates without external synchronization. Our first results demonstrate high field (350 MV/m) acceleration up to 0.8 keV, as well as percent-level energy spread in sub-kiloelecton volt, several tens of fC bunches. These results, which are already suitable for time-resolved low-energy electron diffraction (LEED) experiments, confirm the performance of a THz-driven gun technology that is scalable to relativistic energies [14].

The THz gun [Figs. 1(a)–1(c)] takes the form of a copper parallel-plate waveguide (PPWG) with a subwavelength spacing of 75 μm. We exploit this structure's transverse electromagnetic mode for unchirped, uniform enhancement of the THz field [16]. A free-space vertically polarized THz beam is coupled into the PPWG by a taper. EM simulations [Fig. 2(a)] [17] were utilized to optimize the taper and calculate the coupling efficiency. Inside, a copper film photocathode serves as the bottom plate of the PPWG. There, a UV pulse back-illuminates the film, producing electrons inside the PPWG by photoemission. Concurrently, the THz field accelerates the electrons vertically across the PPWG. The electrons exit the gun through a slit on the top plate (anode) and are spectrally characterized by a retarding field analyzer (RFA) or counted by a Faraday cup. Both UV and THz pulses are generated from the same 1030 nm pump laser, ensuring absolute timing synchronization. See Supplement 1 for more on the gun design/fabrication.

The THz pulse, generated in lithium niobate by the tilted-pulse-front method (Supplement 1), is focused into the gun with

Corrected 1 November 2016

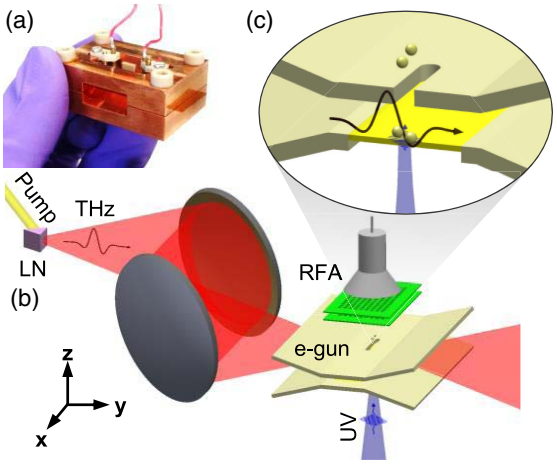

Fig. 1. THz gun concept. (a) Photograph of the THz gun; (b) a single-cycle THz pulse, generated via optical rectification in lithium niobate (LN), is coupled into the THz gun, which takes the form of a parallel-plate waveguide for field confinement. A UV-backilluminated photocathode emits an electron bunch, which is accelerated by the THz field. The bunch exits through a slit on the top plate, and a retarding field analyzer (RFA) measures its energy spectrum. (c) Cross section of the gun, showing the UV-photoemitted electrons accelerated by the THz field and exiting through the slit.

a maximum impinging energy of 35.7 μJ. Electro-optic (EO) sampling at PPWG-center (location of the center of the gun with the gun removed) and PPWG-thru (focus of an image relay following propagation through the PPWG) reveals single-cycle durations of $\tau_{\mathrm{THz}} = 1.2$ ps [Fig. 2(d)], confirming that the PPWG induces minimal dispersion. Figure 2(b) shows the THz beam profile at the free-space focus. Inside the waveguide, the horizontal (x) beam profile remains unaltered, while the vertical (z) profile is distributed uniformly across the 75 μm spacing.

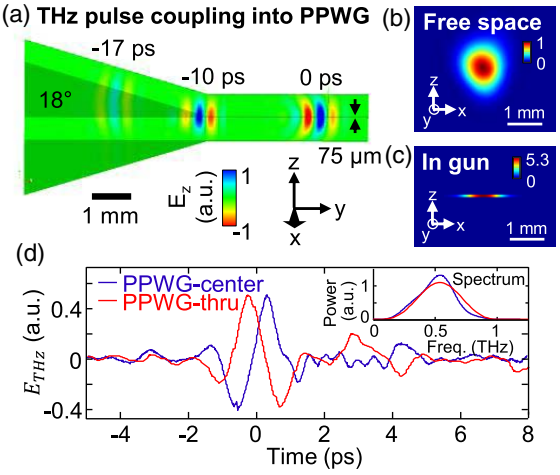

Fig. 2. Design and characterization of the gun. (a) Several snapshots of the single-cycle THz wave coupling into the PPWG, based on EM simulations, (b) THz beam intensity at the free-space focus (measured), (c) THz beam intensity in the gun (calculated; see main text). The colorbars of the two beam profiles show a 5.3 × intensity enhancement in the PPWG. (d) Temporal profiles measured via EO sampling of the THz electric field at PPWG-center and PPWG-thru (scaled) (see main text for definitions). Inset: Power spectrum of the THz beam.

Based on this fact, Fig. 2(c) shows the calculated beam profile inside the gun. Taking into account the energy, waveform, beam profile, and coupling efficiency, the THz pulse has a calculated peak field of 153 MV/m in free space and 350 MV/m in the gun.

The UV emitter pulse, generated by frequency quadrupling of the pump laser (Supplement 1), has a wavelength of 258 nm, an estimated duration of $\tau_{\mathrm{uv}} = 275$ fs (roughly 12.5% of the THz period), and a focused beam waist of 60 μm (x) and 20 μm (y) on the photocathode.

An electron's final momentum gain, p_e, depends on its emission time and can be expressed as $p_e = q\int_{t_{\mathrm{emit}}}^{t_{\mathrm{exit}}} E_{\mathrm{THz}}(t)\mathrm{d}t$, where t_{emit} is the emission time and t_{exit} is the time the electron exits the PPWG. In cases where $t_{\mathrm{exit}} \gg \tau_{\mathrm{THz}}$ (the electron exits long after passage of the THz pulse), p_e can be simplified to $p_e = q\int_{t_{\mathrm{emit}}}^{\infty} E_{\mathrm{THz}}(t)\mathrm{d}t = qA(t_{\mathrm{emit}})$, where $A(t_{\mathrm{emit}})$ is the THz vector potential at the time of emission. To determine the optimum emission time for acceleration, we record the electron energy gain (U_e) spectra and bunch charge (Q) versus delay in Figs. 3(a) and 3(b), respectively. The UV emitter can precede (< – 2 ps), overlap (–2 to 2 ps), or succeed (>2 ps) the THz pulse. In the overlap region (–2 to 2 ps), U_e maps out the phase and amplitude of $A_{\mathrm{THz}}(t_{\mathrm{emit}})$, similar to THz streaking in gases [18]. One exception is that between –0.25 and 0.4 ps, emission occurs in the positive half-cycle of the THz field (opposing Lorentz force), causing a suppression of charge and energy gain. Two delays are selected to be the operating points of the gun. The first delay, $\tau_1 = -2$ ps, produced the highest peak acceleration, while the second delay, $\tau_2 = 0.9$ ps, produced the most monoenergetic spectra. The total bunch charge was 40 fC at τ_1 and 32 fC at τ_2.

When the photoemission precedes the THz pulse (< – 2 ps), a large energy spread centered at ~0.45 keV is observed. The origin of these broadened spectra, enduring for long decay times, is attributed to multiple complex mechanisms encompassing thermal [19] or time-of-flight effects. Further discussion is provided in Supplement 1. When the emission succeeds the THz pulse (>2 ps), there is no net acceleration from that pulse. The constituency of electrons slightly elevated to 50 eV is attributed to the aforementioned decay effects probed by a backreflected THz pulse arriving at 18 ps (also shown in Supplement 1).

In Figs. 3(c) and 3(d), we take a closer look at the energy spectra from the two operating points, τ_1 and τ_2, for three different THz energies, W_{THz}. Each spectrum exhibits a unimodal distribution with an average energy gain increasing with W_{THz}. Except for the $W_{\mathrm{THz}} = 35.7$ μJ spectrum at τ_1, the spectral shapes are asymmetric, with a pedestal toward lower energies and a maximum yield toward higher energies, followed by a sharp cutoff. The high yield near the cutoff indicates that most electrons are emitted at the optimal THz phase and concurrently experience the same acceleration. The pedestal can be attributed to electrons emitted away from the optimal phase, resulting in a lower energy gain. Such dependence of energy gain on emission phase is also evident in RF guns [20].

We continue investigations at τ_1 and τ_2 by plotting U_e versus W_{THz} on a spectrogram, as shown in Figs. 4(a) and 4(b). At both delays, U_e scales mostly linearly with W_{THz} or, equivalently, with E^2_{THz}. This scaling law can be explained by $U_e = \frac{p_e^2}{2m} \propto E^2_{\mathrm{THz}}$, which is valid when $t_{\mathrm{exit}} \gg \tau_{\mathrm{THz}}$. Alternatively, if $t_{\mathrm{exit}} \ll \tau_{\mathrm{THz}}$, the energy gain would be dominated by $U_e = q\int_{z_{\mathrm{emit}}}^{z_{\mathrm{exit}}} E_{\mathrm{THz}}(z)\mathrm{d}z$, leading to a $U_e \propto E_{\mathrm{THz}}$ scaling law, as is typical in RF guns [21]

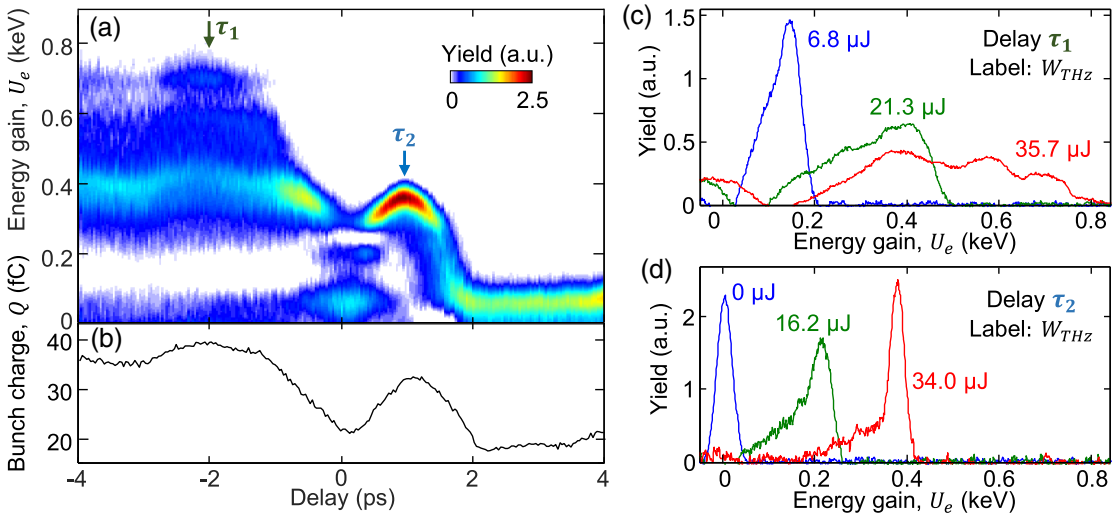

Fig. 3. THz-driven electron energy gain and bunch charge modulation. (a) Measured spectrogram showing the energy gain spectra as a function of delay between UV and THz pulses, at maximum THz energy; (b) measured bunch charge as a function of delay; (c) and (d) electron energy spectra for three different THz energies at delay positions (c) $\tau_1 = -2$ ps and (d) $\tau_2 = 0.9$ ps.

and would be the case in this study for a larger field, reduced PPWG spacing, or relativistic electrons.

At τ_1, increasing the THz energy results in an increase in absolute energy spread [Fig. 4(a)]. Consequently, the relative energy spread, σ_U, remains roughly constant at around 20%–30% [Fig. 4(c)]. The bunch charge increases monotonically with THz energy [Fig. 4(e)]. We obtain a peak energy gain of 0.8 keV at $W_{\mathrm{THz}} = 35.7$ μJ [Fig. 4(a)].

At τ_2, the absolute energy spread remains constant with THz energy [Fig. 4(b)]. Correspondingly, the relative energy spread monotonically decreases with THz energy, to a minimum of 5.8% centered near 0.4 keV [Fig. 4(d)]. The pedestal regions are neglected in the energy spread calculations, since over time those electrons separate from the main bunch. Half of this spread comes from THz shot-to-shot fluctuations (2%), while another large contribution comes from the spread in electron emission time: $\Delta t_{\mathrm{emit}} = \tau_{\mathrm{uv}} = 275$ fs $= \frac{T_{\mathrm{THz}}}{8}$. By stabilizing the laser and shortening τ_{uv} via an optical parametric amplifier [22], the energy spread can be further reduced (see Supplement 1). In Fig. 4(f), the bunch charge increases with THz energy below 7 μJ, indicating that the emission is space charge limited [23]. Above 7 μJ, the bunch charge plateaus, indicating that the THz field overcomes the space charge force and extracts all the emitted electrons.

In Fig. 5(b), we show the calculated single-electron energy gain versus delay, utilizing the shape of the measured THz waveform with a fitted field strength [Fig. 5(a)]. We compare it with the measured peak energy gain from Fig. 3(a). Since the experimentally measured peak energy gain represents the gain of the electron

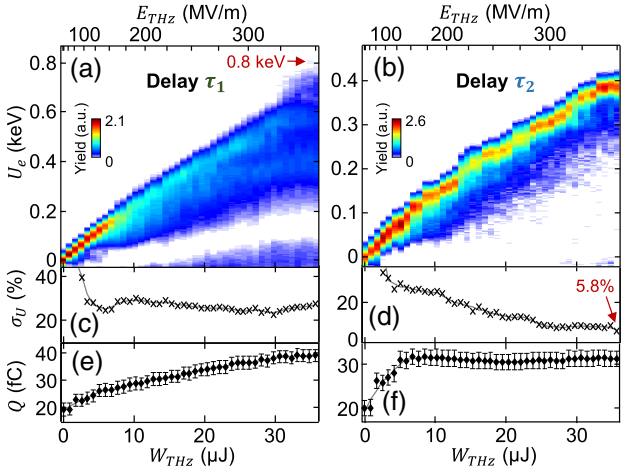

Fig. 4. THz scaling at τ_1 and τ_2; delay positions defined earlier in Fig. 3(a). (a) and (b) Energy gain plotted on a spectrogram to highlight its scaling as a function of accelerating THz energy or THz field. Error bar radius is equal to the absolute RMS energy spread. (c) and (d) Relative RMS energy spread, σ_U, of the accelerated bunch. (e) and (f) Total detected bunch charge exiting the gun, Q. Error bar radius is equal to the RMS instrument noise.

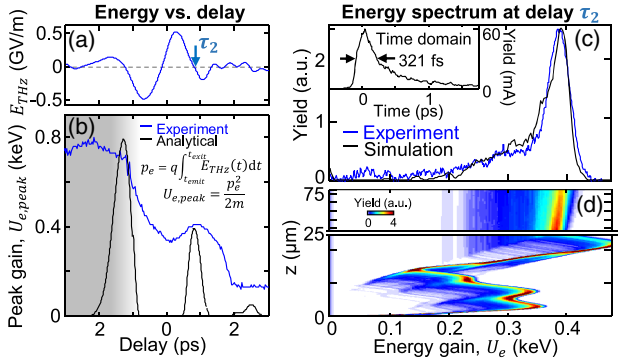

Fig. 5. Numerical analysis of THz gun. (a) THz electric field measured by EO sampling with a fitted field strength; (b) the single-electron energy gain, calculated analytically, is overlaid with the peak energy gain obtained from the experiment in Fig. 3(a); (c) simulated energy spectrum (black line) of the bunch at the gun exit for emission at τ_2, showing excellent agreement with the experiment (blue line). Inset: Temporal profile of the electron bunch at the gun exit, showing a FWHM pulse duration of 321 fs, elongated by space charge. (d) Simulated evolution of the energy spectrum along z. The THz pulse is passed by the time the electrons reach 25 μm.

emitted at the optimal delay and spatial position, comparing it with our analytical expression for single-electron energy gain is justified. Several experimental features are represented in this simple analytical model: (1) a suppression region around 0 ps, (2) relative energy gain levels, and (3) delay between the two peaks. This model provides an alternate method for quantifying the THz field strength inside the gun. Our fitted peak field was 480 MV/m.

To better understand the bunch dynamics under the influence of self-fields and the THz field, the multi-electron particle tracking simulation (Supplement 1) results in Fig. 5(d) show the evolution of the energy spectrum of the 32 fC bunch emitted at τ_2 as it propagates along z. Immediately following emission, the bunch experiences a strong accelerating field, growing in energy to 350 eV over the first 3 μm. During the time that the THz pulse interacts with the bunch (corresponding z distance: 0 to 25 μm), the energy undergoes four acceleration/deceleration cycles, caused by the four oscillation cycles in the THz field following τ_2. The THz pulse is passed by the time the bunch reaches 25 μm, verifying that $t_{\text{exit}} \gg \tau_{\text{THz}}$, and the bunch drifts to the exit while continuing to experience energy spreading due to space charge forces. At the gun exit ($z_{\text{exit}} = 75$ μm), the simulated energy spectrum has excellent overlap with the experimental spectrum [Fig. 5(c)]. The sharp cutoff, pedestal height, pedestal length, and central lobe width are all reproduced flawlessly by the model. The simulated temporal profile at the gun exit [Fig. 5(c) inset] exhibits a pulse duration of 321 fs, longer than the initial 275 fs due to space charge. All the numerical analyses incorporated space charge, imitated the experimental conditions, and used the THz field profile shown in Fig. 5(a).

In conclusion, we demonstrated high-field (>300 MV/m), quasi-monoenergetic (few percent spread) THz acceleration of several tens of fC electron bunches to sub-kiloelectron volt energies in an ultracompact, robust device. No degradation in performance was observed over 1 billion shots. While the operating pressure was 40 μTorr, no change in performance was observable up to 10 mTorr. This first result of a jitter-free, all-optical THz gun, powered by a few-millijoule laser, performs in accordance with underlying simulations and is encouraging for future developments. In its current state, it can be used for time-resolved LEED [24]. Further improvements on the gun structure and THz field promise relativistic electrons [14].

Funding. European Research Council (ERC) (Synergy 609920); Air Force Office of Scientific Research (AFOSR) (A9550-12-1-0499); Deutsche Forschungsgemeinschaft (DFG) (EXC1074, SOLSTICE:SPP1840); National Defense Science and Engineering Graduate (NDSEG) Fellowship; Alexander von Humboldt-Stiftung Fellowship.

Acknowledgment. We thank Andrej Berg, Thomas Tilp, and Johann Derksen (engineering support), Wenjie Lu (coatings), Richard Temkin (measurement equipment), Prasahnt Sivarajah (EO sampling support), and Stuart Hayes and Erich Ippen (productive technical discussions). W. R. Huang was supported in part by a NDSEG Fellowship and X. Wu by an Alexander von Humboldt-Stiftung Fellowship.

See Supplement 1 for supporting content.

REFERENCES

1. H. Wiedemann, *Particle Accelerator Physics* (Springer, 2007).
2. F. Loehl, I. Bazarov, S. Belomestnykh, M. Billing, E. Chojnacki, Z. Conway, J. Dobbins, B. Dunham, R. Ehrlich, M. Forster, S. M. Gruner, C. Gulliford, G. Hoffstaetter, V. Kostroun, M. Liepe, Y. Li, X. Liu, H. Padamsee, D. Rice, V. Shemelin, E. Smith, K. Smolenski, M. Tigner, V. Veshcherevich, and Z. Zhao, in *Proceedings of 1st International Particle Accelerator Conference (IPAC'10)* (2010), p. 45.
3. F. Zhou, C. Adolphsen, Y. Ding, Z. Li, and A. Vlieks, in *Proceedings of 1st International Particle Accelerator Conference (IPAC'10)* (2010), p. 1761.
4. V. Dolgashev, S. Tantawi, Y. Higashi, and B. Spataro, Appl. Phys. Lett. **97**, 171501 (2010).
5. L. Laurent, S. Tantawi, V. Dolgashev, C. Nantista, Y. Higashi, M. Aicheler, S. Heikkinen, and W. Wuensch, Phys. Rev. ST Accel. Beams **14**, 041001 (2011).
6. G. J. H. Brussaard, A. Lassise, P. L. E. M. Pasmans, P. H. A. Mutsaers, M. J. Van Der Wiel, and O. J. Luiten, Appl. Phys. Lett. **103**, 141105 (2013).
7. M. Harmand, R. Coffee, M. R. Bionta, M. Chollet, D. French, D. Zhu, D. M. Fritz, H. T. Lemke, N. Medvedev, B. Ziaja, S. Toleikis, and M. Cammarata, Nat. Photonics **7**, 215 (2013).
8. W. J. Engelen, M. A. van der Heijden, D. J. Bakker, E. J. D. Vredenbregt, and O. J. Luiten, Nat. Commun. **4**, 1693 (2013).
9. E. A. Peralta, K. Soong, R. J. England, E. R. Colby, Z. Wu, B. Montazeri, C. McGuinness, J. McNeur, K. J. Leedle, D. Walz, E. B. Sozer, B. Cowan, B. Schwartz, G. Travish, and R. L. Byer, Nature **503**, 91 (2013).
10. E. A. Nanni, W. R. Huang, K.-H. Hong, K. Ravi, A. Fallahi, G. Moriena, R. J. D. Miller, and F. X. Kärtner, Nat. Commun. **6**, 8486 (2015).
11. J. Zawadzka, D. A. Jaroszynski, J. J. Carey, and K. Wynne, Appl. Phys. Lett. **79**, 2130 (2001).
12. A. J. Goers, G. A. Hine, L. Feder, B. Miao, F. Salehi, J. K. Wahlstrand, and H. M. Milchberg, Phys. Rev. Lett. **115**, 194802 (2015).
13. W. R. Huang, E. A. Nanni, K. Ravi, K.-H. Hong, A. Fallahi, L. J. Wong, P. D. Keathley, L. E. Zapata, and F. X. Kärtner, Sci. Rep. **5**, 14899 (2015).
14. A. Fallahi, M. Fakhari, A. Yahaghi, M. Arrieta, and F. X. Kärtner, Phys. Rev. Accel. Beams **19**, 081302 (2016).
15. M. Shalaby and C. P. Hauri, Nat. Commun. **6**, 5976 (2015).
16. K. Iwaszczuk, A. Andryieuski, A. Lavrinenko, X.-C. Zhang, and P. U. Jepsen, Opt. Express **20**, 8344 (2012).
17. A. Fallahi and F. X. Kärtner, J. Phys. B **47**, 234015 (2014).
18. U. Fruhling, E. Plo, M. Krikunova, R. Kalms, F. Budzyn, and O. Grimm, Nat. Photonics **3**, 523 (2009).
19. G. Herink, L. Wimmer, and C. Ropers, New J. Phys. **16**, 123005 (2014).
20. K. J. Kim, Nucl. Instrum. Methods Phys. Res. A **275**, 201 (1989).
21. J. R. Harris, K. L. Ferguson, J. W. Lewellen, S. P. Niles, B. Rusnak, R. L. Swent, W. B. Colson, T. I. Smith, C. H. Boulware, T. L. Grimm, P. R. Cunningham, M. S. Curtin, D. C. Miccolis, D. J. Sox, and W. S. Graves, Phys. Rev. Accel. Beams **14**, 053501 (2011).
22. L. D. Ziegler, J. Morais, Y. Zhou, S. Constantine, M. K. Reed, M. K. Steiner-Shepard, and D. Lommel, IEEE J. Quantum Electron. **34**, 1758 (1998).
23. J. Rosenzweig, N. Barov, S. Hartman, M. Hogan, S. Park, C. Pellegrini, G. Travish, R. Zhang, P. Davis, G. Hairapetian, and C. Joshi, Nucl. Instrum. Methods Phys. Res. A **341**, 379 (1994).
24. M. Gulde, S. Schweda, G. Storeck, M. Maiti, H. K. Yu, A. M. Wodtke, S. Schäfer, and C. Ropers, Science **345**, 200 (2014).